Triple differential cross sections for the electron-impact ionization of H_2 molecules for equal and unequal outgoing electron energies

J. Colgan,[1] O. Al-Hagan,[2] D. H. Madison,[2] C. Kaiser,[3] A. J. Murray,[3] and M. S. Pindzola[4]
[1]*Theoretical Division, Los Alamos National Laboratory, Los Alamos, New Mexico 87545, USA*
[2]*Department of Physics, Missouri University of Science and Technology, Rolla, Missouri 65409, USA*
[3]*School of Physics and Astronomy, University of Manchester, Manchester M13 9PL, United Kingdom*
[4]*Department of Physics, Auburn University, Auburn, Alabama 36849, USA*
(Received 26 March 2009; published 15 May 2009)

A comprehensive theoretical and experimental investigation of the triple differential cross sections arising from the electron-impact ionization of molecular hydrogen is made, at an incident electron energy of 35.4 eV, for cases where the outgoing electrons have equal and unequal energies, and for a range of experimental geometries. Generally, good agreement is found between two theoretical approaches and experiment, with the best agreement arising for intermediate geometries with large gun angles and for the perpendicular geometry.

DOI: 10.1103/PhysRevA.79.052704 PACS number(s): 34.80.Dp

I. INTRODUCTION

Studies of the electron-impact ionization of one- and two-electron systems have provided a wealth of information about the role of electron-electron correlation, polarization, and three-body effects in the ionization process [1]. As experimental techniques such as recoil-ion momentum spectroscopy and multielectron coincidence detection have become ever more sophisticated, the triple differential cross sections (TDCSs) for electron-impact ionization have been measured for a wide variety of electron angles and energies, and now for many different targets (see for example [2–10]). Recent theoretical progress in several nonperturbative approaches now mean that good agreement with measurement for a variety of kinematical conditions exists. For example, for the electron-impact ionization of atomic hydrogen, theory and experiment are in excellent agreement for all possible differential cross sections [11–16], and for the ionization of helium [17–20] a somewhat similar situation exists.

This progress has spurred recent measurements of the TDCS arising from ionization of the hydrogen molecule [21–23], which have mainly been made at quite high incident electron energies, in order to test perturbative plane-wave and distorted-wave theoretical approaches [24]. Other distorted-wave approaches employing an average over all molecular orientations have been used to examine the TDCS arising from the ionization of N_2 and H_2 [25–30]. Some of these theoretical approaches have also been extended to examine the triple differential cross sections arising from the electron-impact ionization of the hydrogen molecule at much lower incident energies (35.4 eV), where the correlation between the electrons can be expected to play a more prominent role. For example, recent distorted-wave [31] and time-dependent close-coupling (TDCC) [32] calculations have found good agreement with measurements for the TDCS from ionization of H_2 for equal-energy sharing of the outgoing electrons.

In this paper, we present further comparisons of these approaches with measurements made using the Manchester experimental apparatus [2,3,33] at an incident electron energy of 35.4 eV, and present calculations and measurements of the TDCS for *unequal*-energy-sharing conditions for the outgoing electrons. In the following section we give outlines of the two theoretical approaches (molecular distorted-wave theory and time-dependent close-coupling theory) used to compute the TDCS. This is followed by a brief overview of the experimental setup used in the measurements presented here. We then discuss in detail the results and comparisons between theory and experiment. We end with a short conclusion.

II. THEORETICAL APPROACH

A. 3DW theory

The three-body distorted-wave (3DW) model has been described elsewhere [25–29], so only a brief outline of the theory will be presented. The TDCS for 3DW is given by

$$\frac{d^3\sigma}{d\Omega_a d\Omega_b dE_b} = \frac{1}{(2\pi)^5}\frac{k_a k_b}{k_i}|T|^2, \tag{1}$$

where $\vec{k}_i$, $\vec{k}_a$, and $\vec{k}_b$ are the wave vectors for the initial, scattered, and ejected electrons, respectively. The scattering amplitude is given by

$$T = \langle \chi_a^-(\vec{k}_a,\mathbf{r}_1)\chi_b^-(\vec{k}_b,\mathbf{r}_2)C_{scat-eject}(r_{12}^{ave})|V - U_i|\phi_j^{OA}(\mathbf{r}_2)\chi_i^+(\vec{k}_i,\mathbf{r}_1)\rangle, \tag{2}$$

where r_1 and r_2 are the coordinates of the incident and the bound electrons, χ_i, χ_a, and χ_b are the distorted waves for the incident, scattered, and ejected electrons, respectively, and $\phi_j^{OA}(\mathbf{r}_2)$ is the initial bound-state wave function which is the orientation-averaged molecule wave function for H_2 [27]. The factor $C_{scat-eject}(r_{12}^{ave})$ is the average Coulomb-distortion factor and V is the initial-state interaction potential between the incident electron and the neutral molecule.

The molecular distorted waves are calculated using a spherically averaged distorting potential as described previously [25–29]. The Schrödinger equation for the incoming electron wave function is given by

$$\left(T + U_i - \frac{k_i^2}{2}\right)\chi_i^+(\vec{k}_i, \mathbf{r}) = 0, \tag{3}$$

where T is the kinetic-energy operator. The initial-state distorting potential U_i contains three components $U_i = U_S + U_E + U_{CP}$, where U_S is the initial-state spherically symmetric static potential, U_E is the exchange potential of Furness and McCarthy [34], which approximates the effect of the continuum electron exchanging with the bound electrons in the molecule, and U_{CP} is the correlation-polarization potential of Perdew and Zunger [35,36]. The static potential U_S has two parts, the electronic potential $V_{ele}(r)$ and the nuclear potential $V_{nuc}(r)$,

$$U_S(r) = V_{ele}(r) + V_{nuc}(r). \tag{4}$$

Here $V_{ele}(r)$ is obtained by taking a spherical average of the interaction of the projectile electron with the molecular electrons using a numerical Hartree-Fock charge distribution calculated for the molecular electrons. The nuclear potential $V_{nuc}(r)$ is the interaction between the incident electron and two protons separated by $1.4a_0$, averaged over all orientations. This spherical average places a charge of +2 uniformly distributed on a sphere of radius $0.7a_0$. The final-state distorted waves are calculated in the same manner except that the charge distribution for an ion is used to calculate the distorting potentials.

In previous works for higher incident energy electrons [23,27,30], the full Coulomb-distortion factor $C(r_{12})$ was used in the T matrix [Eq. (2)], where r_{12} is the actual relative electron-electron separation which ranges from 0 to infinity in the evaluation of the T-matrix integral. However, for lower energies of interest in this study, it became clear that using $C(r_{12})$ overestimated the effect of the final-state electron-electron repulsion, normally called the post-collision interaction (PCI). Consequently, we have used the Ward-Macek average C factor [37], which gave better agreement with the experimental results.

B. Time-dependent close-coupling method

The TDCC technique [38] is also used to obtain the triple differential cross sections for the ionization of H_2. This approach has been used previously to obtain total cross sections for electron-impact ionization of H_2^+ [39] and H_2 [40], and was recently shown to produce good agreement for triple differential cross sections for equal-energy sharing [32]. We expand the total electronic wave function for the two outgoing electrons as products of four-dimensional radial angular functions and rotational functions [39] using

$$\Psi^M(\vec{r}_1, \vec{r}_2, t) = \sum_{m_1, m_2} \frac{P^{l_0 MS}_{m_1 m_2}(r_1, \theta_1, r_2, \theta_2, t)}{r_1 r_2 \sqrt{\sin\theta_1}\sqrt{\sin\theta_2}} \Phi_{m_1}(\phi_1)\Phi_{m_2}(\phi_2), \tag{5}$$

where $M = m_1 + m_2$ and $\Phi(\phi) = \frac{e^{im\phi}}{\sqrt{2\pi}}$ in center-of-mass spherical polar coordinates. The angular reduction of the time-dependent Schrödinger equation then yields a set of time-dependent close-coupled partial differential equations given by

$$\begin{aligned} i\frac{\partial P^{l_0 MS}_{m_1 m_2}(r_1, \theta_1, r_2, \theta_2, t)}{\partial t} &= T_{m_1 m_2}(r_1, \theta_1, r_2, \theta_2) P^{l_0 MS}_{m_1 m_2}(r_1, \theta_1, r_2, \theta_2, t) \\ &+ \sum_{m_1' m_2'} V^M_{m_1 m_2, m_1' m_2'}(r_1, \theta_1, r_2, \theta_2) P^{l_0 MS}_{m_1' m_2'}(r_1, \theta_1, r_2, \theta_2, t), \end{aligned} \tag{6}$$

where detailed expressions for the single-particle operators $T_{m_1 m_2}(r_1, \theta_1, r_2, \theta_2)$ and the two-particle coupling operator $V^M_{m_1 m_2, m_1' m_2'}(r_1, \theta_1, r_2, \theta_2)$ can be found in [40]. The single-particle operator includes a Hartree-Slater potential term which defines the interaction with the nonionized (frozen) electron. This potential term includes a direct and local exchange potential [40].

The initial condition at time $t = 0$ for the radial angular functions is given by

$$\begin{aligned} P^{l_0 MS}_{m_1 m_2}(r_1, \theta_1, r_2, \theta_2, t = 0) &= \sqrt{\tfrac{1}{2}}[P_{1s0}(r_1, \theta_1) G_{k_0 l_0 M}(r_2, \theta_2)\delta_{m_1, 0}\delta_{m_2, M} \\ &+ (-1)^S G_{k_0 l_0 M}(r_1, \theta_1) P_{1s0}(r_2, \theta_2)\delta_{m_1, M}\delta_{m_2, 0}], \end{aligned} \tag{7}$$

where S is the total spin of the two-electron pair, and the Gaussian wave packet $G_{k_0 l_0 M}$ is a function of the incident energy $k_0^2/2$ and the incident angular momentum l_0. The radial angular orbitals $P_{nlm}(r, \theta)$ are obtained through diagonalization of the one-electron Hamiltonian [40]. The time-dependent close-coupled equations described by Eq. (6) are then propagated in time for each value of M, S, and l_0, until the interaction is complete. As previously discussed [39], an implicit algorithm is used for efficient time evolution.

After propagation to a suitable time T, probabilities for ionization may be obtained [40] by projection onto bound wave functions and appropriate subtraction from unity. An alternative approach is to project directly onto suitable products of H_2^+ continuum functions using

$$\begin{aligned} P^{l_0 MS}_{l_1 m_1 l_2 m_2}(k_1, k_2, T) &= \int dr_1 \int d\theta_1 \int dr_2 \int d\theta_2 P^*_{k_1 l_1 |m_1|}(r_1, \theta_1) P^*_{k_2 l_2 |m_2|}(r_2, \theta_2) \\ &\times P^{l_0 MS}_{m_1 m_2}(r_1, \theta_1, r_2, \theta_2, T), \end{aligned} \tag{8}$$

where $P_{klm}(r, \theta)$ are appropriately normalized H_2^+ continuum functions. This latter approach allows triple differential cross sections to be computed [32] using

$$\frac{d^3\sigma}{dE_1 d\Omega_1 d\Omega_2} = \frac{\pi}{4k_0^2}\frac{1}{k_1 k_2}\sum_S (2S+1) \times \int dk_1 \int dk_2 \delta\left(\alpha - \tan^{-1}\frac{k_2}{k_1}\right)|\mathcal{M}|^2, \tag{9}$$

where k_1 and k_2 are the outgoing electron momenta (ejected into solid angles $\Omega_{1,2}$). For diatomic molecules, where the z axis is defined along the internuclear direction and the in-

coming electron beam is oriented at angles (θ_k, ϕ_k) with respect to the z axis,

$$\mathcal{M} = \sum_{l_0} \sum_{M=-l_0}^{+l_0} i^{l_0} Y^*_{l_0 M}(\theta_k, \phi_k) \sum_{l_1, l_2} \sum_{m_1 m_2} (-i)^{l_1+l_2} e^{i(\sigma_{l_1}+\sigma_{l_2})} \times P^{l_0 MS}_{l_1 m_1 l_2 m_2}(k_1, k_2, T) Y_{l_1 m_1}(\hat{k}_1) Y_{l_2 m_2}(\hat{k}_2) \delta_{m_1+m_2, M}. \tag{10}$$

In Eq. (10), $Y_{lm}(\hat{k})$ is a spherical harmonic, and σ_l is the Coulomb phase shift. Our TDCS expression defined by Eqs. (9) and (10) is given in the molecular frame. To compare with experiment, a transformation must be made into the Laboratory frame. Singly differential cross sections in outgoing electron energy may also be extracted if necessary. Our calculations were performed using a $384 \times 32 \times 384 \times 32$ lattice for the $(r_1, \theta_1, r_2, \theta_2)$ spherical polar coordinates, with a uniform mesh spacing of $\Delta r = 0.2$ a.u. and $\Delta\theta = 0.031\,25\pi$, for all l_0, M values from 0 to 6, and for $S = 0, 1$. The wave functions for $-M$ values were assumed equal to those for $+M$ values, which was confirmed by several explicit calculations for selected $-M$ values. The ranges of l_0, M employed were found to be sufficient to converge all the TDCS presented here, although larger values may be required to fully converge TDCS at larger incident energies. Since the orientation of the molecule with respect to the incoming electron gun angle is *unknown*, we compute the TDCS for all possible molecular angles (θ_N, ϕ_N) (which are the angles made by the molecule with respect to the z axis in the Laboratory frame, where in the Laboratory frame the z axis is defined by the incoming electron-beam direction) and then average over these to compare with the measurements.

III. EXPERIMENTAL SETUP

The apparatus used to collect these data has been well documented [41,42] and so will only be described briefly here. The electron source is comprised of an unselected energy electron gun which uses two electrostatic lenses to focus a collimated electron beam onto the interaction region. The energy of the incident electron beam can be changed from ~20 eV to 300 eV, while maintaining a beam angle of zero degrees and a pencil angle of $\pm 2°$. Typical electron-beam currents used in these experiments ranged from 200 to 1000 nA, as detected on a Faraday cup. The electron energy analyzers are of a hemispherical design, the input to these analyzers being focused onto the interaction region using a three-element cylindrical electrostatic lens with an acceptance angle of $\pm 3°$. Electrons of the correct selected energy are detected and amplified using X719BL channel electron multipliers, whose output is fed to ORTEC 473A constant fraction discriminators (CFDs) via Philips scientific 6954 preamplifiers. The output NIM pulses from the CFDs are fed to an ORTEC time-to-amplitude converter (TAC), one output being time delayed so as to produce a coincidence signal within the timing window of the TAC. The output from the TAC feeds a multichannel analyzer (MCA) which accumulates the correlated coincidence counts from the experiment.

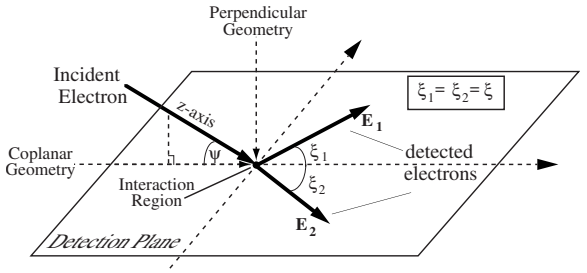

FIG. 1. The experimental geometry. The incident electron beam makes an angle ψ with respect to the detection plane defined by the analyzers. $\psi = 0°$ defines a coplanar geometry, $\psi = 90°$ a perpendicular geometry. The analyzers rotate through angles ξ_1 and ξ_2 as shown. In the current experiments $\xi_1 = \xi_2$. A common normalization point exists for all gun angles when $\xi_1 = \xi_2 = 90°$.

The two electron analyzers are located on separate turntables inside the vacuum system so as to rotate around a detection plane with angles ξ_1 and ξ_2, as shown in Fig. 1. The electron gun can also be moved through an angle ψ with respect to the detection plane. When $\psi = 0°$ the electron gun lies in the detection plane which is referred to as a *coplanar geometry*, whereas when $\psi = 90°$ the incident electron beam is orthogonal to the detection plane, referred to as the *perpendicular geometry*. A common point occurs between all geometries when $\xi_1 = \xi_2 = 90°$, and this allows all data to be normalized to this common reference point at any given energy.

The interaction region must be precisely positioned at the center of rotation of the analyzers and the electron gun. This is facilitated using laser diodes to accurately define the axes of these components, which are adjusted using custom built in-vacuum translators [43,44]. The molecular hydrogen beam effuses from a 1 mm diameter platinum-iridium needle located ~6 mm from the interaction region which rotates with the electron gun. The background pressure inside the chamber is 2×10^{-7} torr, which increases to 1.2×10^{-5} torr while the experiment is operating. Typical electron counts from the analyzers range from 20 to 2 kHz depending on the angles of the analyzers and gun, whereas the coincidence count rates range from ~2 Hz to ~0.01 Hz.

The experiments proceed by selecting a gun angle ψ, then moving the analyzers to a given angle $\xi_1 = \xi_2 = \xi$ before collecting data (typically for 2000 s at each angle ξ). The analyzers are then moved to new angles, and the experiment is repeated until the analyzers have covered the available detection plane. The possible detection angles are limited by the physical size of the analyzers, electron gun, and Faraday cup. The experiment continues for a set gun angle ψ until the statistical variation in the accumulated data is small. This may take up to 20 sweeps of the detection plane, depending upon the coincidence count rates. Once a set of data is accumulated for a given geometry, the gun is moved to a new angle and the process is repeated. All data are then placed on a common scale by equating the results at the common normalization point given by $\xi_1 = \xi_2 = 90°$.

Control of the experiment is facilitated using custom-designed control software which not only adjusts the angles of the detectors and gun, but also optimizes the signal by

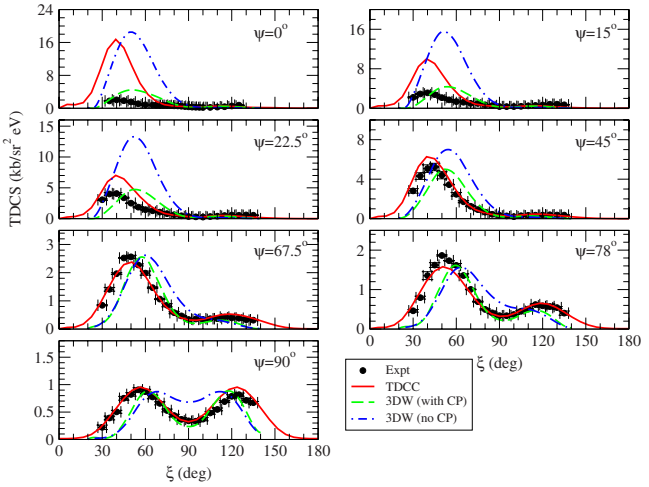

FIG. 2. (Color online) Triple differential cross sections for the electron-impact ionization of H_2 for equal-energy sharing between the outgoing electrons ($E_1=E_2=10$ eV). We present cross sections for various values of the gun angle ψ, as a function of the angle ξ, where 2ξ is the angle between the outgoing electrons. The measurements are compared with TDCC calculations and two sets of 3DW calculations; one including a correlation-polarization potential [labeled 3DW (with CP)] and one without this potential [labeled 3DW (no CP)]. Both sets of 3DW calculations are divided by 6.3 to allow a better comparison with the other results. 1 kb=1.0 $\times 10^{-21}$ cm^2; 1 kb/sr^2 eV $\approx 1\times 10^{-3}$ a.u.

computer controlling the voltages on the analyzers and electron gun [45]. In this way the experiment automatically adjusts for any long term drifts in the operating conditions of the apparatus over the several weeks required for data accumulation.

IV. RESULTS AND DISCUSSION

A. Equal-energy sharing

We begin our discussion by presenting, in Fig. 2, TDCS for ionization of H_2 for equal-energy-sharing outgoing electrons. A selection of these results have previously been presented [31,32]. We compare the experimental data to TDCC calculations and two 3DW calculations: one including a correlation-polarization potential (CP) [labeled 3DW (with CP)] and one without [labeled 3DW (no CP)]. The relative measurements are normalized to the absolute TDCC calculations at $\psi=\xi=90°$, and the common point which exists at $\xi=90°$ for all ψ values (confirmed in all the calculations) allows the measurements to be relatively normalized. This choice of normalizing the measurements to the TDCC calculations at $\psi=\xi=90°$ gives best overall fit to the complete data set. In all the results presented below, the 3DW calculations have been scaled (as specified in the figure captions) to the TDCC to provide an equivalent shape and relative magnitude comparison with experimental data. The need for such a scaling is not unexpected as distorted-wave approaches often differ significantly from measurements of the total ionization cross section [40] at low and intermediate incident energies.

The most obvious trend from the comparisons in Fig. 2 is that experiment and theory are in good agreement when considering the shape of the TDCS for large ψ values. In particular, the TDCC and 3DW (with CP) calculations are in very good agreement with experiment for the perpendicular geometry ($\psi=90°$). This trend persists as ψ decreases down to 45°, with the 3DW (with CP) calculations predicting a binary peak at slightly larger ξ values than found in the experiment and TDCC calculations. The 3DW (no CP) calculations also compare reasonably well with experiment for ψ values from 45° to 90°, but are perhaps not in as good agreement as the 3DW (with CP) calculations.

For lower ψ values, the agreement between experiment and all the calculations worsens, with poorest agreement arising for the coplanar $\psi=0°$ case. The 3DW (with CP) calculations are in best agreement with the relative magnitude of the experiment, but again predict binary peak positions at larger ξ values than found experimentally. The TDCC calculations find a similar binary peak position compared to experiment, but predict a much larger TDCS than found experimentally. The 3DW (no CP) calculations have a similar binary peak position compared to the 3DW (with CP) calculations, but, like the TDCC calculations, predict a much larger relative TDCS.

We note also that the experimental data indicate that the largest cross section is found for the $\psi=45°$ case, which is also found in the 3DW (with CP) calculations. However, the TDCC calculations and the 3DW (no CP) calculations both predict that the largest cross section is found in the coplanar geometry. This might suggest that inclusion of the correlation-polarization potential may change the magnitude of the TDCC calculations, but tests show that inclusion of this potential in the TDCC calculations makes almost no difference to the resulting TDCS. Previous experiments [2,3] and calculations [19] which examined the TDCS from He at similar energies and geometries also found that the largest cross section is in the coplanar geometry.

It is difficult to understand why the TDCC calculations should be in such poor agreement with experiment for small ψ values, but in good agreement for larger ψ values. The perpendicular geometry exhibits the smallest cross section, yet displays the best agreement between theory and experiment. Also, the TDCC calculations for each ψ are made from the same set of amplitudes, and so should have the same set of convergence properties, and so it might be expected that the level of agreement would be similar for each ψ angle. The ability to internormalize the set of experimental data using the common point at $\xi=90°$ also rules out any potential problem with normalization of the measurements or in the calculations. One tentative explanation for the discrepancy between experiment and theory found at low ψ values is that, for coplanar geometries, the molecules may be significantly more aligned (with respect to the incoming electron beam) than for near-perpendicular geometries. TDCC calculations for the coplanar case and for molecules oriented along the electron beam [32] do predict a smaller cross section than in the average case. However, it is not at all obvious why the molecules would align with the incident electron beam in the coplanar geometry, but not in out-of-plane geometries, since there are no deliberate mechanisms for alignment of the molecules in the experiment. However we do note that recent experiments on proton scattering from H_2 suggest preferen-

tial orientation of the molecule parallel to the beam direction for large scattering angles [46].

The 3DW calculations are also in closer agreement with the measurements in the perpendicular plane. To scatter into the perpendicular plane, the projectile must undergo a very close collision with the nuclei at small impact parameters [31]. This type of scattering dominates in the perpendicular plane, but is less important as the coplanar geometry is approached, where polarization and exchange effects become relatively more important. The 3DW method treats the projectile-nuclear scattering exactly for the model potential, and so shows good agreement with the measurements made in the perpendicular plane. On the other hand, the 3DW method treats polarization and exchange more approximately, which may explain why poorer agreement exists as the coplanar geometry is approached. The TDCC approach treats exchange between the outgoing electrons in an exact manner, but only treats the exchange with the bound electron approximately (via a local exchange approximation). Although we have found that inclusion of a static polarization term makes little difference, we have not explored the effects of dynamic (time-dependent) polarizability of the core. Such considerations may also explain the discrepancies which exist for the coplanar geometry.

It is also instructive to compare the TDCS found for He at similar outgoing electron energies to those presented in Fig. 2. In the He case, measurements made using the same apparatus [2,3] were previously shown to be in good agreement with convergent close-coupling calculations [19] and are also in good agreement with TDCC and 3DW calculations [47]. The differences between the TDCS from He and from H_2 for the perpendicular geometry have already been discussed in detail [31], and indicate how the TDCS is influenced by the positioning of a nucleus at the center of mass (as in atoms or molecules such as CO_2) compared to diatomic molecules such as H_2. For intermediate geometries, the positions of the binary and recoil peaks are similar for He and H_2, but the recoil peak is generally suppressed more in the H_2 case. This is most clearly demonstrated in the coplanar geometry, where almost no recoil peak is found experimentally or theoretically for H_2, but in the He case the recoil peak has a similar magnitude compared to the binary peak.

B. Unequal-energy sharing

Unequal-energy-sharing TDCS (with one electron having 18 eV and the other 2 eV of the available outgoing energy) are presented in Figs. 3 and 4 for a variety of gun angles ψ. Examining the asymmetric energy sharing case is instructive as it breaks the "doubly symmetric" conditions found for these measurements at equal-energy sharing. Figures 3 and 4 show a similar trend to that found for equal-energy sharing: the best agreement between theory and experiment is found for large ψ values. The TDCC calculations find a binary peak position slightly closer to the experimental position as compared to the 3DW calculations. The agreement between theory and experiment worsens at lower ψ values, but the discrepancies are perhaps not as great as for the equal-energy-sharing case. For the coplanar and low-ψ geometries,

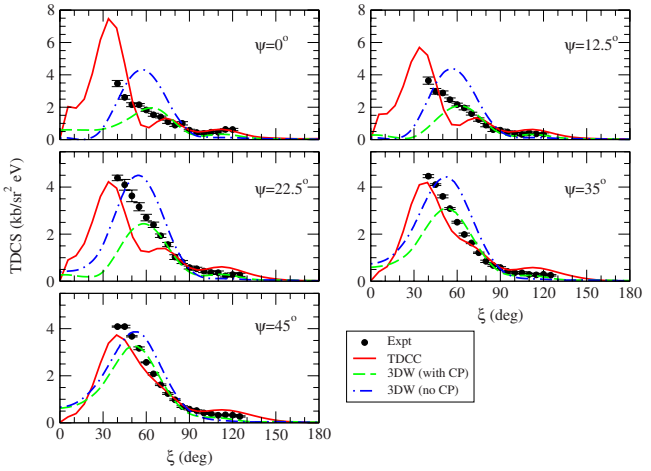

FIG. 3. (Color online) Same as Fig. 2, except for unequal-energy sharing: $E_1=18$ eV; $E_2=2$ eV, for ψ values ranging from 0 to 45 degrees. The 3DW (with CP) cross sections are divided by 3.7 and the 3DW (no CP) cross sections are divided by 4.5 to allow a better comparison with the other results.

the TDCC and 3DW calculations predict somewhat different binary peak positions, although the measurements are such that it is difficult to gauge which set of calculations are in best agreement with the data. The large differences in magnitude of the TDCS are also not as evident for the unequal-energy-sharing case. We also observe that the TDCC calculations predict extra structure in the TDCS for low ψ values, which are not found in the measurements or the 3DW calculations.

The TDCC calculations again find the largest cross section for the coplanar geometry. The experimental data indicates that the largest cross section is found at around $\psi=45°$, although this may be somewhat ambiguous since the measurements could not be made at low enough ξ values to fully map out the binary peak position for low ψ values. However, the 3DW (with CP) calculations also find a maximum for $\psi=45°$, although the drop in the TDCS as ψ is decreased is gradual.

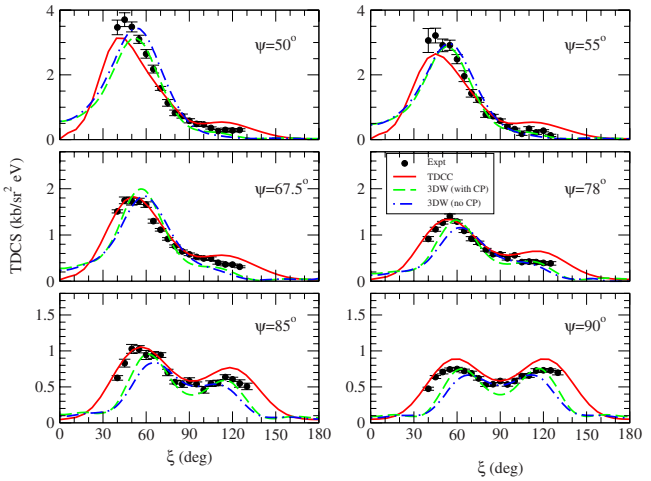

FIG. 4. (Color online) Same as Fig. 3, for ψ values ranging from 50 to 90 degrees.

V. CONCLUSIONS

We have presented a joint experimental and theoretical study of the triple differential cross sections arising from the electron-impact ionization of H_2 at an incident electron energy of 35.4 eV. Results have been presented for both equal ($E_1=E_2=10$ eV) and unequal ($E_1=18$ eV, $E_2=2$ eV) energy sharings, for a variety of experimental geometries, for cases where the molecular orientation is unknown. We find that time-dependent close-coupling (TDCC) calculations and molecular distorted-wave (3DW) calculations give good agreement with measurements for large gun angle values, and especially for the perpendicular geometry. At lower gun angles, and for the coplanar geometry, the agreement between experiment and theory is not as satisfactory. In the 3DW calculations, inclusion of a correlation-polarization potential was found to improve the agreement with experiment, but inclusion of this potential did not alter the TDCC calculations.

In future work, we hope to measure cross sections from molecules oriented with respect to the electron beam. These measurements will test recent predictions of the TDCS for ionization from oriented molecules [32], and may also shed some light on the discrepancies which exist between theory and experiment for the coplanar geometry TDCS as discussed here.

ACKNOWLEDGMENTS

The Los Alamos National Laboratory is operated by Los Alamos National Security, LLC for the National Nuclear Security Administration of the U.S. Department of Energy under Contract No. DE-AC5206NA25396. A portion of this work was performed through DOE and NSF grants to Auburn University. Computational work was carried out at the NCCS in Oak Ridge, TN, and through a LANL Institutional Computing Resources grant. A portion of this work was done under National Science Foundation under Grant No. PHY-0757749, and we acknowledge the EPSRC (U.K.) for additional support to C.K.

[1] E. Weigold and I. E. McCarthy, *Electron Momentum Spectroscopy* (Kluwer, Dordrecht, 1999).
[2] A. J. Murray, M. B. J. Woolf, and F. H. Read, J. Phys. B **25**, 3021 (1992).
[3] A. J. Murray and F. H. Read, J. Phys. B **26**, L359 (1993).
[4] J. Roder, M. Baertschy, and I. Bray, Phys. Rev. A **67**, 010702(R) (2003).
[5] J. Röder, H. Ehrhardt, C. Pan, A. F. Starace, I. Bray, and D. V. Fursa, Phys. Rev. Lett. **79**, 1666 (1997).
[6] A. J. Murray and F. H. Read, Phys. Rev. A **63**, 012714 (2000).
[7] J. G. Childers, K. E. James, M. Hughes, I. Bray, M. Baertschy, and M. A. Khakoo, Phys. Rev. A **68**, 030702(R) (2003).
[8] J. G. Childers, K. E. James, I. Bray, M. Baertschy, and M. A. Khakoo, Phys. Rev. A **69**, 022709 (2004).
[9] M. Dürr, C. Dimopoulou, B. Najjari, A. Dorn, and J. Ullrich, Phys. Rev. Lett. **96**, 243202 (2006).
[10] M. Dürr, C. Dimopoulou, A. Dorn, B. Najjari, I. Bray, D. V. Fursa, Z. Chen, D. H. Madison, K. Bartschat, and J. Ullrich, J. Phys. B **39**, 4097 (2006).
[11] T. N. Rescigno, M. Baertschy, W. A. Isaacs, and C. W. McCurdy, Science **286**, 2474 (1999).
[12] M. Baertschy, T. N. Rescigno, W. A. Isaacs, X. Li, and C. W. McCurdy, Phys. Rev. A **63**, 022712 (2001).
[13] I. Bray, Phys. Rev. Lett. **89**, 273201 (2002).
[14] I. Bray, K. Bartschat, and A. T. Stelbovics, Phys. Rev. A **67**, 060704(R) (2003).
[15] J. Colgan and M. S. Pindzola, Phys. Rev. A **74**, 012713 (2006).
[16] I. Bray, J. Phys. B **33**, 581 (2000).
[17] I. Bray, D. V. Fursa, J. Röder, and H. Ehrhardt, J. Phys. B **30**, L101 (1997).
[18] S. Rioual, J. Röder, B. Rouvellou, H. Ehrhardt, A. Pochat, I. Bray, and D. V. Fursa, J. Phys. B **31**, 3117 (1998).
[19] A. T. Stelbovics, I. Bray, D. V. Fursa, and K. Bartschat, Phys. Rev. A **71**, 052716 (2005).
[20] J. Colgan, M. S. Pindzola, G. Childers, and M. A. Khakoo, Phys. Rev. A **73**, 042710 (2006).
[21] M. Takahashi, N. Watanabe, Y. Khajuria, Y. Udagawa, and J. H. D. Eland, Phys. Rev. Lett. **94**, 213202 (2005).
[22] D. S. Milne-Brownlie, M. Foster, J. Gao, B. Lohmann, and D. H. Madison, Phys. Rev. Lett. **96**, 233201 (2006).
[23] E. M. Staicu-Casagrande, A. Naja, F. Mezdari, A. Lahmam-Bennani, P. Bolognesi, B. Joulakian, O. Chuluunbaatar, O. Al-Hagan, D. H. Madison, D. V. Fursa, and I. Bray, J. Phys. B **41**, 025204 (2008).
[24] C. R. Stia, O. A. Fojón, P. F. Weck, J. Hanssen, and R. D. Rivarola, J. Phys. B **36**, L257 (2003).
[25] J. Gao, D. H. Madison, and J. L. Peacher, J. Chem. Phys. **123**, 204314 (2005).
[26] J. Gao, D. H. Madison, and J. L. Peacher, Phys. Rev. A **72**, 020701(R) (2005).
[27] J. Gao, D. H. Madison, and J. L. Peacher, J. Phys. B **39**, 1275 (2006).
[28] J. Gao, D. H. Madison, and J. L. Peacher, Phys. Rev. A **72**, 032721 (2005).
[29] J. Gao, J. L. Peacher, and D. H. Madison, J. Chem. Phys. **123**, 204302 (2005).
[30] C. Kaiser, D. Spieker, J. Gao, M. Hussey, A. Murray, and D. H. Madison, J. Phys. B **40**, 2563 (2007).
[31] O. Al-Hagan, C. Kaiser, D. Madison, and A. J. Murray, Nat. Phys. **5**, 59 (2008).
[32] J. Colgan, M. S. Pindzola, F. Robicheaux, C. Kaiser, A. J. Murray, and D. H. Madison, Phys. Rev. Lett. **101**, 233201 (2008).
[33] A. J. Murray, J. Phys. B **38**, 1999 (2005).
[34] J. B. Furness and I. E. McCarthy, J. Phys. B **6**, 2280 (1973).
[35] J. P. Perdew and A. Zunger, Phys. Rev. B **23**, 5048 (1981).
[36] N. T. Padial and D. W. Norcross, Phys. Rev. A **29**, 1742 (1984).
[37] S. J. Ward and J. H. Macek, Phys. Rev. A **49**, 1049 (1994).

[38] M. S. Pindzola *et al.*, J. Phys. B **40**, R39 (2007).
[39] M. S. Pindzola, F. Robicheaux, and J. Colgan, J. Phys. B **38**, L285 (2005).
[40] M. S. Pindzola, F. Robicheaux, S. D. Loch, and J. P. Colgan, Phys. Rev. A **73**, 052706 (2006).
[41] A. J. Murray and F. H. Read, Phys. Rev. Lett. **69**, 2912 (1992).
[42] A. J. Murray and F. H. Read, Phys. Rev. A **47**, 3724 (1993).
[43] A. J. Murray, Meas. Sci. Technol. **14**, N72 (2003).
[44] A. J. Murray, M. J. Hussey, and A Venables, Meas. Sci. Technol. **16**, N19 (2005).
[45] A. J. Murray, B. C. H. Turton, and F. H. Read, Rev. Sci. Instrum. **63**, 3346 (1992).
[46] J. S. Alexander, A. C. Laforge, A. Hasan, Z. S. Machavariani, M. F. Ciappina, R. D. Rivarola, D. H. Madison, and M. Schulz, Phys. Rev. A **78**, 060701(R) (2008).
[47] J. Colgan *et al.* (unpublished).